IOP Conf. Series: Materials Science and Engineering **580** (2019) 012010 doi:10.1088/1757-899X/580/1/012010

Following Microstructures during Deformation: In situ X-ray/Neutron Diffraction and HRDIC

E Polatidis[1,2], K Sofinowski[1,3], W-N Hsu[1,3], H Van Swygenhoven[1,3]

[1] Photons for Engineering and Manufacturing Group, Swiss Light Source, Paul Scherrer Institute, Villigen-PSI 5232, Switzerland
[2] Currently: Laboratory for Neutron Scattering and Imaging (LNS), Paul Scherrer Institute, Villigen-PSI 5232, Switzerland
[3] Neutrons and X-rays for Mechanics of Materials, IMX, Ecole Polytechnique Federale de Lausanne, CH-1012 Lausanne, Switzerland

helena.vanswygenhoven@psi.ch

Abstract. The mechanical behavior of three engineering materials is studied employing in situ deformation methods. The study covers metastable austenitic steels with different stacking fault energies during multiaxial loading, a Ti-6Al-4V alloy processed by electron beam melting during uniaxial deformation and a commercial nanocrystalline NiTi alloy during multiaxial deformation. The experimental results obtained by in situ X-ray or neutron diffraction elucidate the load transfer and phase transformation mechanisms, information that is averaged over a relatively large volume containing a statistically representative number of grains. Complementary in situ high resolution digital image correlation allows details to be revealed regarding the localized strain accommodation and slip activity with a sub-grain spatial resolution. It is demonstrated that the synergy of the different length-scale investigations provides a better understanding of the complex relationship between microstructure and deformation behavior in these materials.

1. Introduction

In situ neutron and synchrotron x-ray diffraction are well established techniques for studying internal stress and microstructure evolution [1–3]. The evolution of diffraction peak positions, width and intensity can provide insight on the average intergranular and intragranular strains, and texture evolution within different grain families [4–8], where these grain families are classified according to their crystallographic orientation with respect to the diffraction vector. The average lattice strain of a grain family represents the fraction of applied load, i.e. type-I or macroscopic stresses, shared by that grain family. Elastic anisotropy, plastic slip, grain neighborhood interactions and the direction of loading significantly influence this evolution. In situ diffraction is also particularly useful for studying multi-phase materials during deformation, as it reveals the load transfer between the phases and provides information on the role of each phase for the strain hardening behavior of the composite material. The technique has the advantage of providing average information over relative large volumes that are representative of the studied microstructure. It misses, however, direct spatial microstructure correlations, i.e. observations in individual grains, grain interactions or strain concentrations in particular places.

To have a better link with the microstructure, often electron backscatter diffraction (EBSD) measurements are carried out before and after an in situ deformation and diffraction experiment. Such studies provide additional information on the change of the microstructure in terms of deformation texture, grain refinement or the formation of sub-grain boundaries. However, these observations only reveal the microstructure in stationary states before and after the deformation, and do not provide information on where and how strain is accommodated.

Digital image correlation (DIC) is an optical method that employs tracking and image-registration techniques and is used to follow changes in images. The method is employed in the engineering community for measuring full-field displacement and strains. When applied at higher magnifications, DIC of images obtained during mechanical testing makes it possible to study the localization of plastic deformation on the surface of specimens. Coupling of DIC with scanning electron microscopy (SEM) enables significantly more precise data to be obtained down to the submicron scale [9]. The spatial resolution that can be obtained depends to a great extent on the surface quality of the sample and on the pattern that is used, for instance by using nano-sized microstructural independent patterns such as gold speckle patterns [9] or particles from a colloidal silica suspension [10].

In situ high resolution digital image correlation (HRDIC) can offer a direct link between the microstructure and the strain produced by dislocation slip, twinning and martensitic phase transformations when the evolution during deformation is monitored in the same material portion. Such localized information complements the average information obtained from diffraction techniques. Apart from complimenting macroscopic experimental results, the strain localization obtained by HRDIC can be coupled with crystal plasticity simulations [11].

Here we show that by using a miniaturized multiaxial deformation rig, implementable in an SEM, in situ HRDIC can be carried out to capture the details of the strain hardening mechanisms that are missing to explain the averaged load sharing and the phase transformation behavior obtained by in situ synchrotron X-ray/neutron diffraction techniques. The cases illustrated are the transformation induced plasticity (TRIP) effect in a 304 austenitic steel, the extraordinary hardening behavior in a Ti-6Al-4V alloy processed by electron beam melting (EBM) and the multiaxial mechanical loading behavior of a commercial superelastic NiTi alloy.

2. Methods

2.1. In situ multiaxial deformation

For the in situ multiaxial loading and diffraction experiments, cruciform-shaped samples have been designed with their geometry optimized with the aid of finite element analysis [12]. In situ synchrotron X-ray diffraction experiments have been carried out at the material science beamline (MS) of the Swiss synchrotron (SLS). The miniaturized multiaxial deformation rig [13] or a uniaxial tensile rig [14] are mounted on the goniometer of the powder diffraction station at the MS beamline. The in situ measurements are conducted in transmission mode using a Mythen II microstrip detector with counting time of 30-60 seconds, depending on the material. More details about the experimental setups at the MS beamline and the cruciform sample geometry are given in [14,15].

The multiaxial load rig available at POLDI is used for in situ neutron diffraction studies [16]. The biaxial deformation system is equipped with a 2-camera digital image correlation (DIC) system (GOM, Aramis 5M) for measuring the in-plane strain at the center of the cruciform-shaped sample. Uniaxial loading and equibiaxial loading are performed with a loading rate of 80 N/s. The neutron diffraction measurements are carried out in predefined force intervals after interrupting the loading and holding the displacement. Typically the counting times range from approximately 30 minutes to 120 minutes depending on the required accuracy of the diffraction information. The neutron diffraction data is reduced and fitted using the open source software Mantid [17].

2.2. HRDIC in SEM

For the in situ HRDIC measurements, the miniaturized multiaxial deformation rig is installed inside the chamber of a FEG SEM Zeiss ULTRA 55 [13]. The electron beam with acceleration voltage of 3 kV in

combination with a 20 μm aperture is used for the image acquisition. The images are acquired with an in-lens detector at a working distance of approximately 7.5 mm in order to minimize the topographic contrast by gathering low energy electrons, providing a good signal/noise ratio. SEM images are taken at various magnifications depending on the size of the deformation features to be tracked with a resolution of 3072 × 2304 pixels at the center of the cruciform/dogbone sample after reaching certain strains determined based on the aim of the study. The HRDIC data is analyzed with Ncorr [18], using typically a subset radius of 15 pixels, 0 subset spacing and a strain radius of 3 pixels, determining the circle in which the strain is calculated. Pseudo-strains due to thermal drifts and lens distortion are negligible compared to the strain magnitude observed in e.g. slip bands and therefore, no correction is applied.

2.3. Patterns for DIC

The remodeling of a sputtered gold film can produce nanoscale aggregates of gold particles that can serve as patterns for HRDIC analysis, resulting in strain mapping with sub-micron resolution [9,19]. As a flat and well-polished surface is required in order to achieve good speckle patterns, the NiTi and Ti-6V-4Al samples are ground and polished until a mirror-like surface is achieved. For the 304 steel cruciforms, the novel fabrication process incorporating electrochemical micromachining results in a high-quality surface, ready for direct application of the gold speckle pattern [20]. By adapting the method proposed in [9], fine gold speckle patterns are applied to commercial superelastic NiTi and 304 steel to study the strain accommodation in commercial NiTi and the slip activity in 304 steel under multiaxial deformation. An image of these patterns is shown in figure 1a and figure 1b.

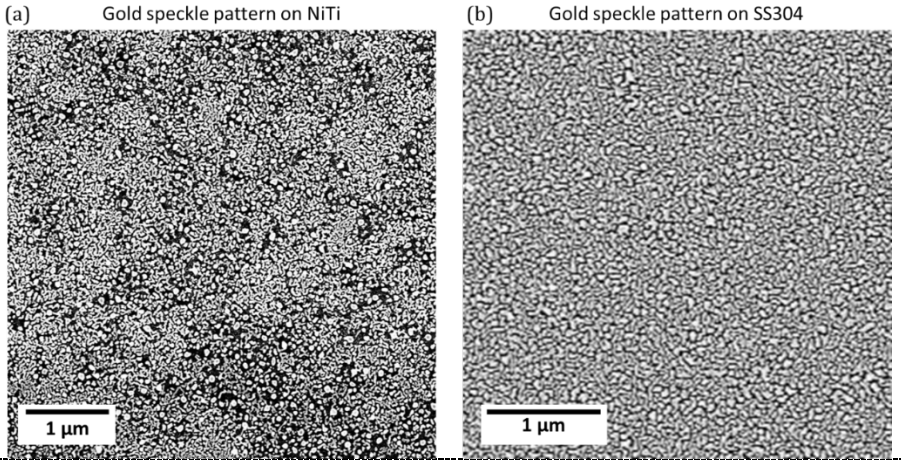

Figure 1. Fine gold speckle patterns allow HRDIC with a sub-micron resolution for (a) commercial superelastic NiTi and (b) austenitic stainless steel 304.

3. Metastable austenitic steels under multiaxial loading

The deformation mechanisms under uniaxial and biaxial load paths were studied in two types of metastable austenitic stainless steels, namely a low staking fault energy (SFE) 201 steel and a medium SFE 304 steel. Both materials are fully austenitic, i.e., have a face-centred cubic crystal structure in the unloaded state and exhibit martensitic phase transformation upon deformation. The evolution of the phases was followed during in situ uniaxial and equibiaxial deformation by neutron diffraction. More details on the experiments are given in [21,22].

In situ neutron diffraction performed on the low SFE 201 steel showed that for the same von Mises strain, more martensite is formed under uniaxial tensile loading than under biaxial tensile deformation. Following the evolution of the neutron diffraction patterns with increasing strain, it is clear that ε-martensite, which has a hexagonal closed packed crystal structure, forms as an intermediate phase prior to the body centered α'-martensite [21]. Post-mortem EBSD investigations show that the majority of the grains under uniaxial deformation favour the formation of ε-martensite, and that the intercepts of the

ε-martensite plates are preferred nucleation sites for α′-martensite. The combined effect of the crystallographic orientation and the load path on the strain-induced martensitic transformation is rationalized as described in the following. The leading and trailing partial dislocations have different Burgers vectors. In low SFE steels for grains with crystallographic orientation such that the leading partial dislocation experiences a higher resolved shear stress than the trailing partial dislocation, the partials separate and form an extensive stacking fault (SF), which allows the local formation of ε-martensite, [23,24].

The opposite behavior is seen for 304 steel, i.e. more martensite is formed under biaxial than under uniaxial deformation [22,25], as apparent by the diffraction peaks corresponding to martensite which appear in figure 2-b, after approximately 15% von Mises strain. Under uniaxial deformation, no diffraction peaks corresponding to martensite are seen until the end of the deformation, at approximately 27% strain, as shown in figure 2-a. Instead, a typical deformation behavior by slip is seen, where a strong <111>-texture forms, parallel to the loading direction, accompanied by significant peak broadening, due to dislocation activity, as seen in figure 2-a. Post mortem EBSD investigations show that the majority of the grains under uniaxial deformation favor the formation of SFs (similarly to 201 steel) which in the case of the higher SFE material, leads to the formation of deformation twinning. A significant number of twins was observed by EBSD in favorably orientated grains under uniaxial deformation [22].

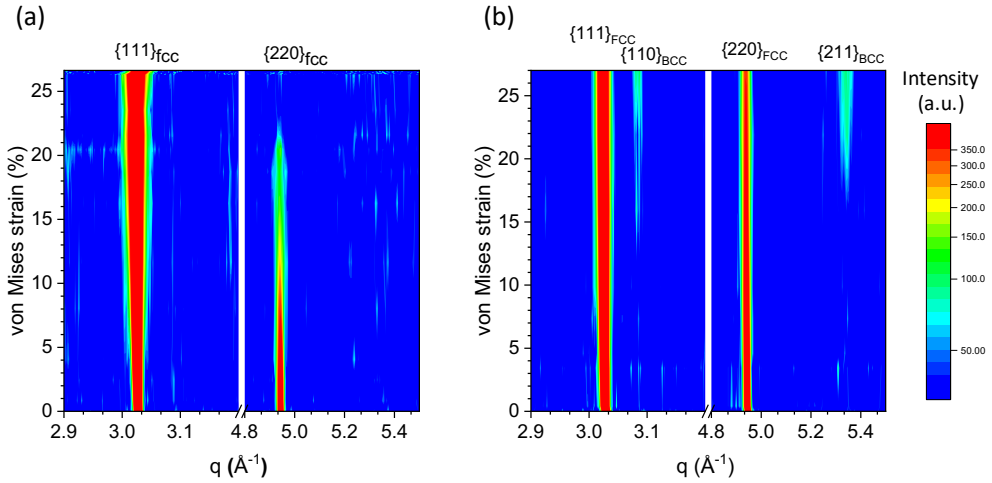

Figure 2. The evolution of the neutron diffracted intensities with increasing strain for a) uniaxial b) equibiaxial tensile deformation of 304 steel. The neutron scattering vector is parallel to the loading direction under uniaxial deformation and parallel with one of the loading axes under equibiaxial deformation.

The interpretation of the different amount of strain-induced α′-martensite under uniaxial and equibiaxial tensile deformation in 201 steel is evident by the suppression or facilitation of the formation of the intermediate phase, i.e. ε-martensite. However, in the medium SFE 304 steel, the formation of deformation twinning and its interaction with the martensite formation is not sufficiently understood to explain the opposite behavior, i.e., why less transformation under uniaxial deformation than under biaxial deformation is observed. Here HRDIC is a particularly useful tool for understanding the interplay between deformation by slip, twinning and martensite formation in these materials, by following the slip activity at the grain level.

Figure 3-a shows an image of the miniaturized cruciform-shaped 304 steel sample and its surface quality. For this study, a novel design for miniaturized cruciform samples was developed where the center of the cruciform is thinned by electrochemical machining (figure 3-a), as described in [20]. The sample surface can be readily used for electron backscatter diffraction (EBSD) and after applying a gold speckle pattern, high resolution digital image correlation (HRDIC) can be carried out.

Thanks to the gold speckle pattern, the evolution of the slip activity within each grain can be followed at different strain levels, as shown in figure 3-b and figure 3-c). Careful examination of 21 grains in each loading state shows that equibiaxial deformation promotes the activation of slip on multiple slip planes in the {111} lattice plane family within each grain, as shown in figure 3-e. Fewer grains with multiple activated slip planes are observed under uniaxial loading (figure 3-d). It is thus concluded that the enhanced twinning under uniaxial tensile deformation retards the activation of slip in secondary slip planes, which in turn results in less martensite nucleation (as a consequence of the reduction in the number of shear band intercepts, which are favorable nucleation sites for martensite formation). In contrast, under equibiaxial tensile deformation, less twinning results in more martensite formation via the activation of slip on more than one slip plane in each grain.

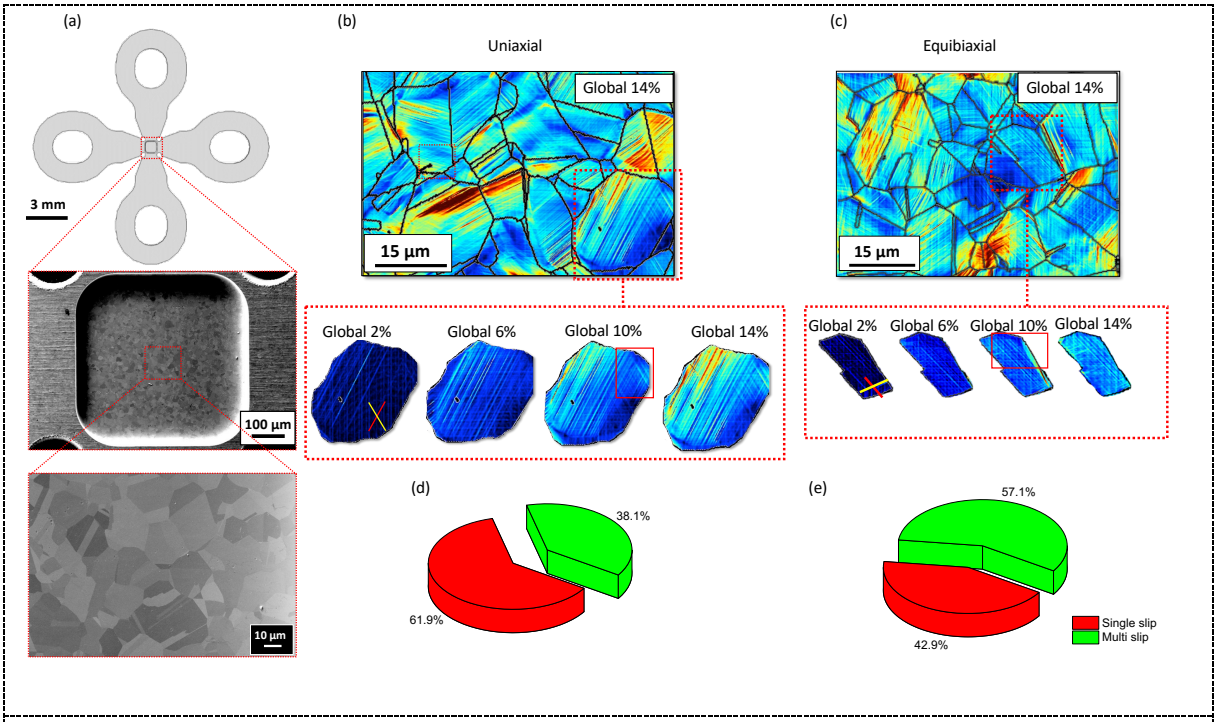

Figure 3. (a) A miniaturized cruciform-shaped 304 steel sample with reduced thickness in the centre, ready to be used for EBSD and HRDIC; (b-c) HRDIC showing slip traces at the grain level during deformation under uniaxial and equibiaxial tensile deformation. The isolated grains (indicated with red squares), show examples where a second slip system is activated. The statistical analysis (percent of grains) shows that less grains exhibit multiple slip under (d) uniaxial than (e) equibiaxial deformation [20].

4. Ti-6Al-4V

The source of high-work hardening behavior was investigated for a Ti-6Al-4V alloy processed by EBM and a novel post heat treatment. The samples were hot isostatic pressed (HIPed), annealed for two hours at sub-β transus temperatures and then water quenched. The resulting microstructure consisted of large α lamellae surrounded by regions of acicular α'-martensite, with the volume fraction of the martensite regions depending on the annealing temperature. A full description of the preparation techniques is provided in [26,27]. The post-treated material exhibits a higher ultimate tensile strength and, in some cases, a higher ductility than the standard dual- phase α+β material obtained in the as-HIPed (no post treatment) condition. This was found to be due to a high work hardening in the post-treated alloy, 2-3 times higher than in the as-HIPed samples [27]. The load sharing between the phases was investigated with in situ XRD at the MS beamline (Swiss Light Source) and the results were corroborated with

transmission electron microscopy (TEM), transmission Kikuchi diffraction (TKD), and in situ HRDIC [28].

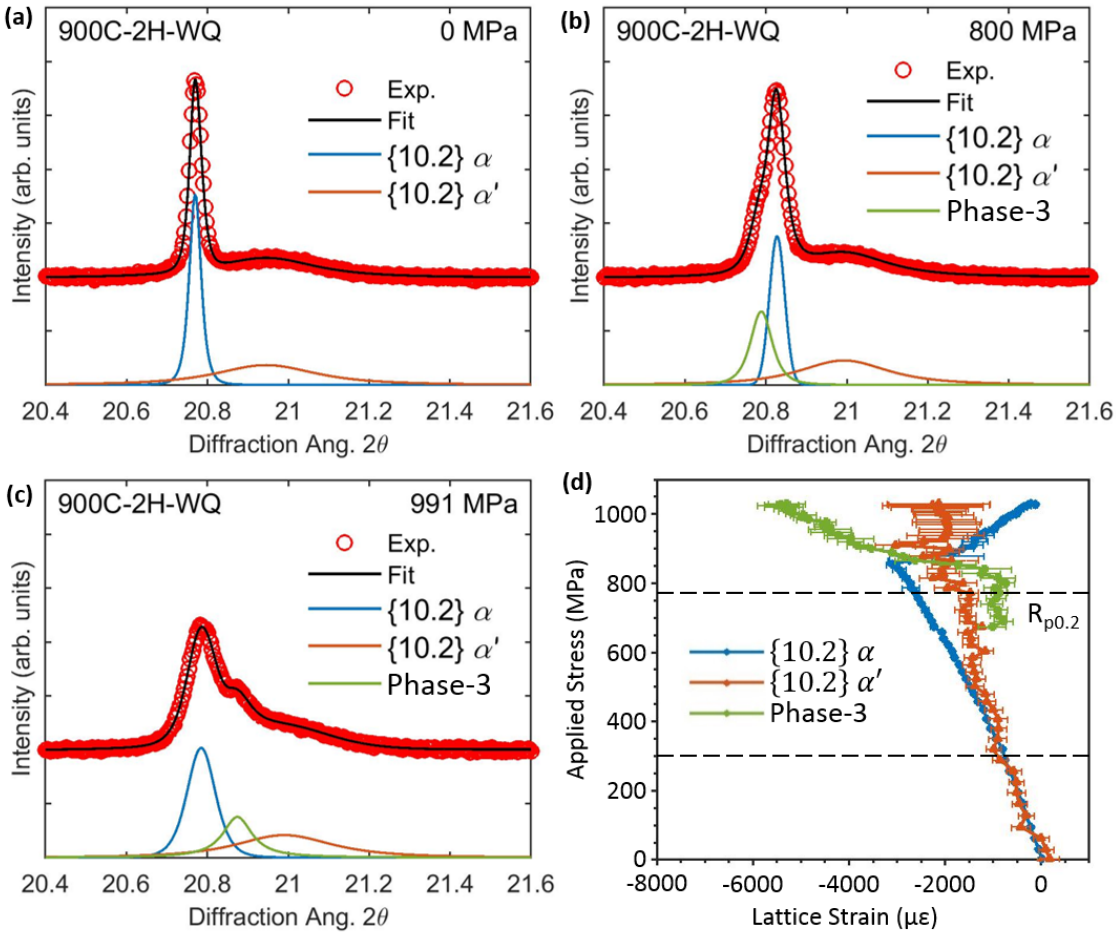

Figure 4. X-ray diffraction of the {10.2} α, {10.2} α', and a Phase-3 peaks for Ti-6Al-4V at (a) 0 MPa (initial, unloaded state), (b) 800 MPa, and (c) 991 MPa,(d) the elastic lattice strain as function of the applied stress(diffraction vector $\boldsymbol{Q}_{\perp}$ perpendicular to the loading direction)

In situ uniaxial tensile loading experiments with XRD revealed the existence of a third phase in the martensitic regions, mechanically distinct from the α and α' phases (figure 4). The XRD peaks of this phase are visible as shoulders at several HCP reflections before loading, and from additional peaks that initially are obscured by nearby α reflections but which appear during loading as the phases take load differently. This is shown in figure 4-a to c. The diffracted peaks could be fit as either a secondary hexagonal closed packed (hcp) phase (secondary α) or an orthorhombic phase (α"-martensite) and could not be identified with full confidence. Therefore, the phase will be henceforth referred to as "Phase-3." The martensitic regions therefore consist of small laths of both α' and Phase-3. They are a few 100 nm long, approximately one order of magnitude smaller than the α lamellae. The deformation is the result of the load-sharing between the three phases, shown in figure 4-d for the peaks near the $\{10.2\}_{hcp}$ reflection of a sample heat treated at 900°C. Note that the diffraction vector **Q** is perpendicular to the loading direction, i.e. the calculated elastic lattice strains measure the Poisson contraction of the grain families. Thus, in figure 4-d, a more negative value of the lattice strain implies that the sample takes more load along the loading direction.

Initially, the sample is in the elastic regime and the elastic lattice strains for all phases evolve linearly. At around 300 MPa, the sample enters a microplastic regime where the elastic lattice strains for α' and Phase-3 deviate from linearity and begin to take less load. The α' peak broadens, suggesting it is deforming plastically, while the peak width of the observable Phase-3 peaks does not change. Load is transferred to the α phase. The onset of microplastic yield corresponds to the onset of plastic deformation in several soft α grain families, which rapidly shed load. The α' grains continue to deform plastically during this regime, and the load is transferred to the harder α grain families and Phase-3, which behaves as the hardest phase. The presence of an additional hard phase allows the α and α' phases to deform plastically beyond what they could in a dual-phase material, resulting in the enhanced work hardening and ductility.

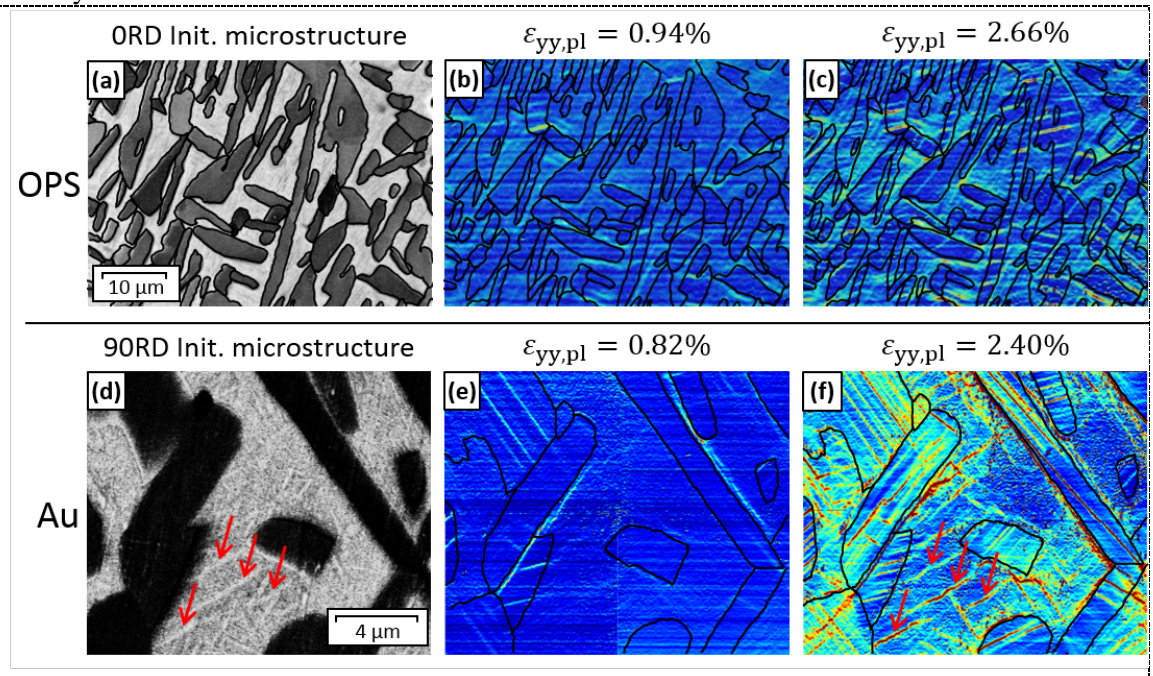

Figure 5. In situ HRDIC of (a,b,c) OPS and (d,e,f) gold speckle pattern on Ti-6Al-4V (heat treated at 900°C). Initial microstructures are backscatter electron images. Dark grains are α lamellae, light gray regions are martensitic regions. Grain boundaries are drawn manually as a guide for the eye.

To better understand the composite behavior of the martensitic regions, in situ HRDIC was performed during uniaxial tensile loading. Dogbone-shaped samples were deformed inside of an SEM and paused at various points during loading to collect highly magnified images of the sample surface. Two types of samples, one coated with OPS and one coated with gold speckles, were tested to examine the strain partitioning at two length scales. The strain maps are shown in figure 5. HRDIC confirmed that, as expected from the XRD, strain was accommodated first within the martensite regions. Additionally, the images show that the strain is not evenly distributed within the martensite regions. Rather, strong strain concentrations form along the interfaces between the α lamellae and martensite regions (figure 5-a) and within the martensite regions themselves (figure 5-b). The strain concentrations between the martensite regions and α lamellae form very early in the deformation and imply that the α lamellae are delaminating due to the mechanical differences between them. Delamination explains how Phase-3 could shed load without deforming plastically in the microplastic regime. After microplastic yield, strain concentrations are observed at the interfaces of the larger laths within the martensite regions themselves (figure 5-b). This confirms the composite behavior of the martensite regions, which, prior to these experiments, were thought to be homogeneous. Strain concentrations at the interfaces grow and form microcracks, which ultimately lead to fracture of the samples. The in situ mechanical results imply

that varying the post-treatment annealing temperature can tune the volume fraction of the martensite regions and the size of the laths within them to optimize work hardening and ductility.

5. Strain accommodation in commercial superelastic NiTi

Superelasticity of NiTi allows it to sustain large strain without introducing permanent deformation owing to the reversible martensitic transformation. The B2 austenite phase transforms into the B19' martensite phase upon loading. Once the external load is removed, martensite can transform back to austenite. The transformation behavior in the commercial superelastic nanocrystalline NiTi (Memry GmbH) was studied by combining cruciform multiaxial deformation tests with in situ synchrotron X-ray diffraction. Details about the sample geometries and experimental setups are given in reference [15].

Figure 6 shows the evolution of the diffraction reflections in a selected 2θ range during a "square" load path change. The initial microstructure is full austenite phase, as evidenced by the presence of reflections only corresponding to the B2 phase before loading. During uniaxial loading along the F1 direction, austenite transforms into martensite when a critical transformation force (~24 N) is reached. The intensity of $\{110\}_{B2}$ drops drastically, while the martensite reflections $\{002\}_{B19'}$ and $\{012\}_{B19'}$ appear. Subsequent loading along the F2 direction does not introduce new martensite reflections but shows a slight decrease in the B19' volume fraction, suggesting that a reverse transformation is induced by changing the load path. Upon unloading along the F1 direction (changing loading condition from F1F2 to F2max), the martensite reflections formed at F1max, $\{002\}_{B19'}$ and $\{012\}_{B19'}$, decrease in intensity and eventually disappear. Meanwhile new martensite reflections, $\{110)_{B19'}$ and $\{020\}_{B19'}$, appear and grow in intensity. Different sets of martensite reflections corresponding to different loading directions suggest a dependency of the martensitic variant selection on the load path, which is also reported in [29], where uniaxial and equibiaxial loads result in different martensite footprints in diffraction spectra. The final unloading of F2 induces a complete reverse transformation from martensite to austenite. Upon unloading, the strong $\{110\}_{B2}$ appears again, and no martensite reflection is retained. In situ X-ray diffraction clearly demonstrates the path dependency of the martensite variants during the load path change in the commercial NiTi.

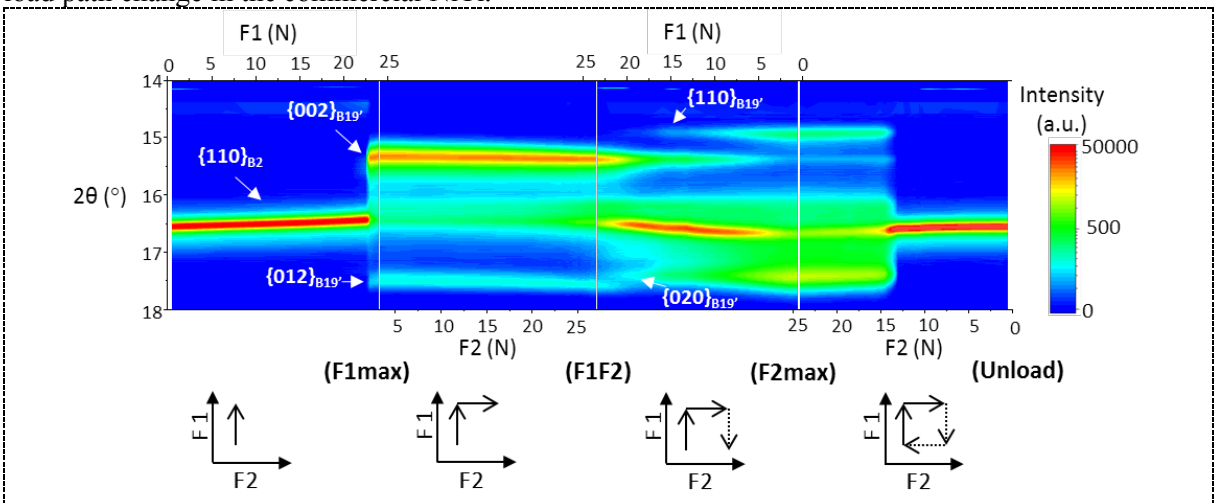

Figure 6. Evolution of the diffraction intensity of different reflections during a square load path change in NiTi alloy.

As characterized by EBSD, the initial austenite microstructure is complex (see figure 7-a). The large austenite grains delineated with dashed line in figure 7-a contain bands varying in width, direction and crystallographic orientation. High-magnification EBSD and TEM reveal that these bands consist of agglomerations of subgrains (average crystallite size: 40 nm) having similar crystallographic orientations. In order to correlate the transformation behavior observed by in situ X-ray diffraction with

the complex microstructure, in situ HRDIC using gold speckle pattern applied on the surface of the cruciform-shape sample is performed. More experimental details are given in [15].

Figure 7-b shows the in-plane strain maps at F1max and F2max during the square load path. Note that the field of view for HRDIC is the same as the EBSD map shown in figure 7-a. HRDIC shows a non-uniform strain distribution inside the large austenite grains, suggesting that the strain accommodated by the phase transformation is microscopically heterogeneous. Depending on the loading direction, the high-strain traces appear in different places in the same large austenite grains. For instance, in Grain A, different inclinations and locations of the high-strain traces can be observed under F1max and F2max. The high-strain traces mostly orient similarly to the band structure shown in the EBSD crystallographic orientation map, underlying the importance of the initial austenite microstructure on the transformation behavior. A careful inspection of the behavior in different grains confirms the important role of the austenite subgrain structure [15]. Together with the in situ diffraction data shown in figure 6, the link between the austenite microstructure and the transformation behavior during the square load path change is uncovered. The martensitic transformation occurs in the nanoscaled austenite subgrains. Depending on the loading direction, different groups of subgrains transform collectively into different sets of martensitic variants, hence producing the heterogeneous strain distributions observed in the HRDIC maps.

After one cycle of the square load path change, diffraction data shows a full austenite phase and slight peak broadening in austenite reflections, which implies the formation of dislocations. The HRDIC strain map taken after unloading (figure 7-c) shows residual strain traces, which correspond to the sharp contrast features in electron channeling contrast image (ECCI). These results affirm the formation of dislocations during a single load path change cycle.

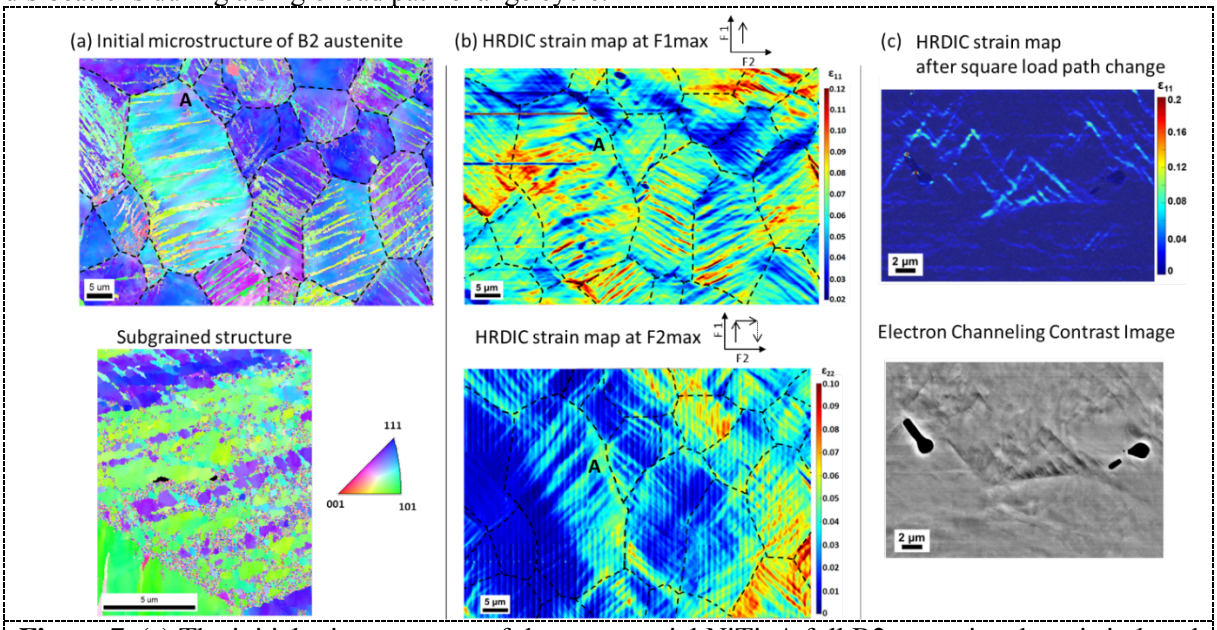

Figure 7. (a) The initial microstructure of the commercial NiTi. A full B2 austenite phase is indexed with EBSD. The subgrains are revealed in a higher magnification map. (b) The HRDIC strain map taken at F1max and F2max during the square load path change. (c) The HRDIC strain map and the electron channeling contrast image taken at the same area, after fully unloading.

6. Summary

Three examples have been presented to highlight the complementary aspects of HRDIC and in situ diffraction methods for investigating the mechanical behavior of engineering materials. Neutron diffraction showed that in a 304 austenitic steel the martensitic transformation is enhanced during equibiaxial deformation. HRDIC provided the additional understanding that under biaxial loading more grains exhibit multiple slip systems, and hence more nucleation sites for martensite are provided. For

the Ti-6Al-4V alloy processed by EBM, in situ XRD revealed a rather complex load sharing between three mechanically distinct phases, whereas HRDIC demonstrated an inhomogeneous strain accommodation and delamination between very fine laths. Together the results of the two techniques explain why this composite microstructure exhibits a high work hardening with good ductility. Finally, synchrotron XRD showed that in a commercial NiTi alloy different martensite variants appear during a strain path change, while HRDIC revealed how this strain is accommodated and underlined the role of the nano-sized subgrain structure on the mechanical behavior of these material.

Acknowledgements
The authors thank the European Research Council for the ERC advanced Grant MULTIAX (339245).

References
[1] Clausen B 1997 *Characterisation of polycrystal deformation by numerical modelling and neutron diffraction measurements* (Roskilde: Risø National Laboratory)
[2] Oliver E C 2002 The generation of internal stresses in single and two phase materials *PhD Thesis*
[3] Oliver E C, Daymond M R and Withers P J 2004 Interphase and intergranular stress generation in carbon steels *Acta Mater*. **52** 1937–51
[4] Hutchings M T, Withers P J, Holden T M and Lorentzen T 2005 *Introduction to the Characterization of Residual Stress by Neutron Diffraction* (CRC Press)
[5] Dawson P, Boyce D, MacEwen S and Rogge R 2001 On the influence of crystal elastic moduli on computed lattice strains in AA-5182 following plastic straining *Mater. Sci. Eng. A* **313** 123–44
[6] Wong S L and Dawson P R 2010 Influence of directional strength-to-stiffness on the elastic–plastic transition of fcc polycrystals under uniaxial tensile loading *Acta Mater*. **58** 1658–78
[7] Van Swygenhoven H and Van Petegem S 2013 In-situ mechanical testing during X-ray diffraction *Mater. Charact*. **78** 47–59
[8] Upadhyay M V, Capek J, Van Petegem S, Lebensohn R A and Van Swygenhoven H 2017 Intergranular Strain Evolution During Biaxial Loading: A Multiscale FE-FFT Approach *JOM* **69** 839–47
[9] Di Gioacchino F and da Fonseca J Q 2013 Plastic strain mapping with sub-micron resolution using digital image correlation *Exp. Mech*. **53** 743–754
[10] Yan D, Tasan C C and Raabe D 2015 High resolution in situ mapping of microstrain and microstructure evolution reveals damage resistance criteria in dual phase steels *Acta Mater*. **96** 399–409
[11] Tasan C C, Hoefnagels J P M, Diehl M, Yan D, Roters F and Raabe D 2014 Strain localization and damage in dual phase steels investigated by coupled in-situ deformation experiments and crystal plasticity simulations *Int. J. Plast*. **63** 198–210
[12] Upadhyay M V, Panzner T, Van Petegem S and Van Swygenhoven H 2017 Stresses and Strains in Cruciform Samples Deformed in Tension *Exp. Mech*. **57** 905–20
[13] Van Petegem S, Guitton A, Dupraz M, Bollhalder A, Sofinowski K, Upadhyay M V and Van Swygenhoven H 2017 A Miniaturized Biaxial Deformation Rig for in Situ Mechanical Testing *Exp. Mech*. **57** 569–80
[14] Van Swygenhoven H, Schmitt B, Derlet P M, Van Petegem S, Cervellino A, Budrovic Z, Brandstetter S, Bollhalder A and Schild M 2006 Following peak profiles during elastic and plastic deformation: A synchrotron-based technique *Rev. Sci. Instrum*. **77** 013902
[15] Hsu W-N, Polatidis E, Šmíd M, Casati N, Van Petegem S and Van Swygenhoven H 2018 Load path change on superelastic NiTi alloys: In situ synchrotron XRD and SEM DIC *Acta Mater*. **144** 874–83
[16] Van Petegem S, Wagner J, Panzner T, Upadhyay M V, Trang T T T and Van Swygenhoven H 2016 In-situ neutron diffraction during biaxial deformation *Acta Mater*. **105** 404–16

[17] Arnold O, Bilheux J C, Borreguero J M, Buts A, Campbell S I, Chapon L, Doucet M, Draper N, Ferraz Leal R, Gigg M A, Lynch V E, Markvardsen A, Mikkelson D J, Mikkelson R L, Miller R, Palmen K, Parker P, Passos G, Perring T G, Peterson P F, Ren S, Reuter M A, Savici A T, Taylor J W, Taylor R J, Tolchenov R, Zhou W and Zikovsky J 2014 Mantid—Data analysis and visualization package for neutron scattering and μ SR experiments *Nucl. Instrum. Methods Phys. Res. Sect. Accel. Spectrometers Detect. Assoc. Equip.* **764** 156–66

[18] Blaber J, Adair B and Antoniou A 2015 Ncorr: Open-Source 2D Digital Image Correlation Matlab Software *Exp. Mech.* **55** 1105–22

[19] Scrivens W A, Luo Y, Sutton M A, Collette S A, Myrick M L, Miney P, Colavita P E, Reynolds A P and Li X 2007 Development of Patterns for Digital Image Correlation Measurements at Reduced Length Scales *Exp. Mech.* **47** 63–77

[20] Polatidis E, Hsu W-N, Šmíd M and Van Swygenhoven H 2019 A High Resolution Digital Image Correlation Study under Multiaxial Loading *Exp. Mech.* **59** 309-317

[21] Polatidis E, Hsu W-N, Šmíd M, Panzner T, Chakrabarty S, Pant P and Van Swygenhoven H 2018 Suppressed martensitic transformation under biaxial loading in low stacking fault energy metastable austenitic steels *Scr. Mater.* **147** 27–32

[22] E. Polatidis, M. Smid, W.-N. Hsu, M. Kubenova, J. Capek, T. Panzner and H. Van Swygenhoven The interplay between deformation mechanisms in austenitic 304 steel during uniaxial and equibiaxial loading, under review, Materials Science and Engineering A.

[23] Byun T S 2003 On the stress dependence of partial dislocation separation and deformation microstructure in austenitic stainless steels *Acta Mater.* **51** 3063–71

[24] Martin S, Wolf S, Martin U, Krüger L and Rafaja D 2016 Deformation Mechanisms in Austenitic TRIP/TWIP Steel as a Function of Temperature *Metall. Mater. Trans. A* **47** 49–58

[25] Zecevic M, Upadhyay M V, Polatidis E, Panzner T, Van Swygenhoven H and Knezevic M 2019 A crystallographic extension to the Olson-Cohen model for predicting strain path dependence of martensitic transformation *Acta Mater.* **166** 386–401

[26] de Formanoir C, Michotte S, Rigo O, Germain L and Godet S 2016 Electron beam melted Ti–6Al–4V: Microstructure, texture and mechanical behavior of the as-built and heat-treated material *Mater. Sci. Eng. A* **652** 105–19

[27] de Formanoir C, Brulard A, Vivès S, Martin G, Prima F, Michotte S, Rivière E, Dolimont A and Godet S 2017 A strategy to improve the work-hardening behavior of Ti–6Al–4V parts produced by additive manufacturing *Mater. Res. Lett.* **5** 201–8

[28] Karl Sofinowski, Miroslav Šmíd, Ivo Kuběna, Solange and Vivès, Nicola Casati, Stéphane Godet, Helena Van Swygenhoven In Situ Characterization of a High Work Hardening Ti-6Al-4V prepared by Electron Beam Melting *Under review, Acta Materialia*

[29] Hsu W-N, Polatidis E, Šmíd M, Van Petegem S, Casati N and Van Swygenhoven H 2019 Deformation and degradation of superelastic NiTi under multiaxial loading *Acta Mater.* **167** 149–58